

A variational-difference numerical method for designing progressive-addition lenses[☆]



Wei Jiang^{a,b,*}, Weizhu Bao^c, Qinglin Tang^c, Hanquan Wang^d

^a School of Mathematics and Statistics, Wuhan University, Wuhan 430072, PR China

^b Beijing Computational Science Research Center, Beijing 100084, PR China

^c Department of Mathematics and Center for Computational Science and Engineering, National University of Singapore, Singapore 119076, Singapore

^d School of Statistics and Mathematics, Yunnan University of Finance and Economics, Kunming 650221, PR China

HIGHLIGHTS

- We propose a variational-difference numerical method for designing progressive-addition lenses.
- The method can be very easily understood and implemented by optical engineers.
- The method can provide satisfactory designs for optical engineers in several seconds.
- The method can be a powerful candidate tool for designing various free-form lenses.

ARTICLE INFO

Article history:

Received 26 February 2013

Accepted 31 October 2013

Keywords:

Progressive-addition lens

Variational-difference method

Linearization

Background surface

Functional minimization problem

ABSTRACT

We propose a variational-difference method for designing the optical free form surface of progressive-addition lenses (PALs). The PAL, which has a front surface with three important zones including the far-view, near-view and intermediate zones, is often used to remedy presbyopia by distributing optical powers of the three zones progressively and smoothly. The problem for designing PALs could be viewed as a functional minimization problem. Compared with the existing literature which solved the problem by the B-spline finite element method, the essence of the proposed variational-difference numerical method lies in minimizing the functional directly by finite difference method and/or numerical quadratures rather than in approximating the solution of the corresponding Euler–Lagrange equation to the functional. It is very easily understood and implemented by optical engineers, and the numerical results indicate that it can produce satisfactory designs for optical engineers in several seconds. We believe that our method can be a powerful candidate tool for designing various specifications of PALs.

© 2013 Elsevier Ltd. All rights reserved.

1. Introduction

When we reach about forty years old, the natural process of aging begins to affect our vision, and the lens of our eyes thickens and progressively loses its flexibility to the point where we have trouble focusing on near points. This causes presbyopia. Therefore, it is natural that people with presbyopia need their vision to be corrected by wearing spectacle lenses. People can often use single-vision lenses to correct this problem. However, although these can enable very good vision for nearby regions, people need to take

them off in order to have good vision for distance regions. To avoid this inconvenience, more complicated lenses such as the bifocal lens, trifocal lens and progressive-addition lens (PAL) have been designed.

Bifocal lenses, which were first invented by Benjamin Franklin in 1784 because he suffered from poor vision at that time, can be divided into two parts, the top half for viewing at distance and the bottom half for reading; trifocal lenses are made up of three parts, with the addition of a part for viewing at intermediate region. A major drawback for these two kinds of lenses is the vision jump when the eyes move from seeing far-distance to near-distance objects. PALs, also known as no-line bifocal lenses, can remove the vision jump drawback. Fig. 1 shows a schematic illustration of PALs. As shown in Fig. 1(a), a PAL has a front surface with three different view zones, including distance-view (i.e. far-view), near-view and intermediate zones. More precisely, a PAL has a large far-vision area with low refractive optical power in

[☆] This paper has been recommended for acceptance by Vadim Shapiro.

* Corresponding author at: School of Mathematics and Statistics, Wuhan University, Wuhan 430072, PR China. Tel.: +86 18062622728; fax: +86 27 68752256.

E-mail addresses: jiangwei1007@gmail.com (W. Jiang), matbaowz@nus.edu.sg (W. Bao), tqtlq12010@gmail.com (Q. Tang), hanquan.wang@gmail.com (H. Wang).

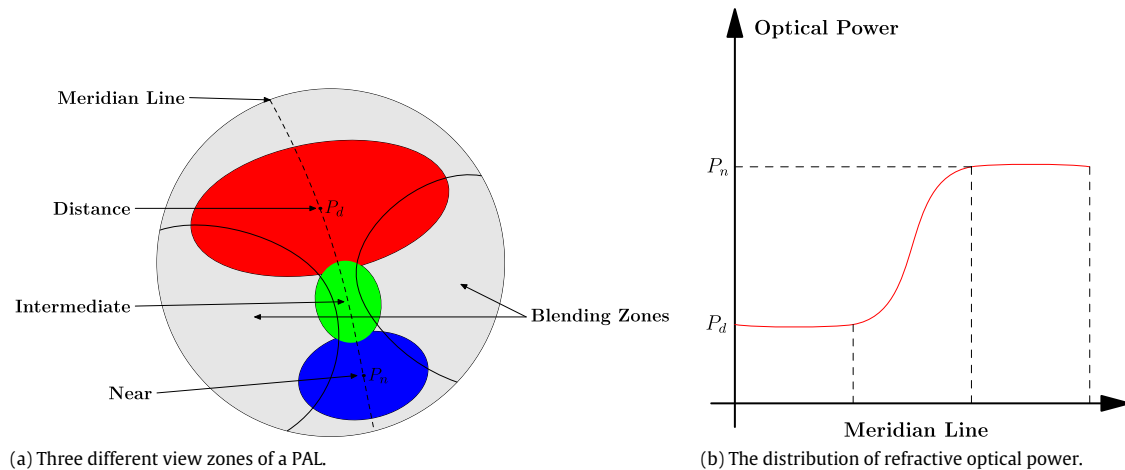


Fig. 1. Schematic illustration of a PAL.

the upper part and a small near-vision area with high refractive optical power in the lower part, while an intermediate vision area where the optical power varies progressively and smoothly is used to connect with the upper and lower parts of the PAL. Fig. 1(b) shows a typical distribution of refractive optical power on the three different view zones of a PAL along the meridian line. In general, a good PAL design requires that the optical power on the far-view, near-view and intermediate zones be progressively and smoothly changed according to every patient's prescription, and that the astigmatism on the three zones be as small as possible simultaneously. However, the remaining parts, which are called as blending zones shown in Fig. 1(a), also inevitably have astigmatism because of the prescribed power distribution along the three zones. Although the blending zones are the least frequently used by spectacle wearers, the astigmatism will bring them a bad visual feeling and make them uncomfortable. Therefore, a good PAL design also needs to require that the blending zones have relatively low astigmatism.

As early as 1907, British optometrist Owen Aves made a prototype design for PALs [1,2]. His design idea came from the shape of elephant's trunk, which consisted of a conical back surface and a cylindrical front with opposing axes in order to create a power progression. This design was the prototype of modern PALs, but it was not commercialized at that time. Since the invention of the first modern design and entry into the marketplace around the 1960s, PALs have been gradually accepted by worldwide customers due to their ability to eliminate the vision jump line between the far-view and near-view portions of the lens and offer spectacle wearers a smooth transition between different vision zones. Nowadays, PALs have gained worldwide acceptance as the high-performance spectacle lenses used in the correction of presbyopia and currently account for more than half of all multi-focal lens sales. Although early progressive lens designs have had great success in providing presbyopic patients with more comfortable vision, lens designers seem to be approaching a limiting state [3]. Because the visual requirements of spectacle lens wearers vary greatly from person to person, it has been understood for some time that the traditional "one-size-fits-all" progressive lens design framework is no longer suitable for every progressive lens wearer. Therefore, designers need to tailor more suitable and specialized spectacle lenses by considering the unique visual requirements of the individual progressive lens wearer. Thus, the advances in design methods are becoming ever more significant for designing the next generation PALs.

Designing PALs is often regarded as a very complicated mathematical problem [4–10]. In general, the design methods can be

divided into two categories, direct methods and indirect methods. In a direct method, such as the research work of Winthrop [4,5] and Baudart, Ahsbahs and Miege [6], the refractive optical power is first assigned along a line called the meridian line (shown in Fig. 1) on the lens, then the surface on the lens is generated from the meridian line by prescribing curves which are transverse to it. The shapes of these curves are chosen to have the desired surface curvature on the meridian line. However, the performance of such design methods is often less than satisfactory because there is no effective control over the distribution of the astigmatism. For the indirect method, such as the method proposed by Loos et al. [7,8], the lens design can be simplified as an optimization problem or a functional minimization problem. In such a method, a cost function (functional), which attempts to balance between reaching the desired distribution of refractive optical power and the unwanted astigmatism, will be devised and beforehand given. The design objective is to minimize the cost function (functional) by numerical methods. The indirect method is often more effective and powerful, and it can be quickly implemented by powerful computer simulations. It can also provide more precise control for the distribution of the optical power and astigmatism on the lens surface. Therefore, it represents a powerful candidate tool for designing the customized PALs.

In this paper, we focus on the indirect methods for designing PALs. Based on a functional minimization mathematical model, we propose an efficient variational-difference numerical method for solving the problem. Compared with the existing literature which solved the problem by the *B*-spline finite element method [7,9,10], the essence of the proposed variational-difference numerical method lies in minimizing the functional directly by the finite difference method rather than in approximating the solution of the corresponding Euler–Lagrange equation to the functional. It is very easily understood and implemented by optical engineers, and its memory and computational costs are smaller than that of the *B*-spline finite element method. Our numerical results indicate that it could produce satisfactory design results for optical engineers in several seconds.

The rest of the paper is organized as follows. In the next section, we briefly present a mathematical model based on a quadratic functional minimization problem for designing PALs. In Section 3, a variational-difference numerical method is proposed for solving the quadratic functional minimization problem. In Section 4, numerical results are presented to demonstrate the high performances of the proposed numerical method. Finally, Section 5 concludes the paper with a summary and future research plans.

2. Mathematical models

2.1. Functional minimization problem

For the design of PALs, the optical power is one of the two crucial design parameters for optical engineers according to every patient's prescription. In general, the optical power of PAL is determined by the shapes of the front and back surfaces, together with the material properties of the lens. In ophthalmic optics, the optical power P of a lens can be expressed in terms of [7,9,10]

$$P = (1 - n)P^b + \frac{(n - 1)P^f}{1 - d(1 - \frac{1}{n})P^f}, \quad (2.1)$$

where P^b and P^f are the mean curvatures of the back and front surfaces, respectively, d is the thickness of the lens and n represents the refractive index of the lens material. Under the assumption that the lens is very thin, we obtain an approximate formula from (2.1) by setting $d = 0$:

$$P = (n - 1)(P^f - P^b). \quad (2.2)$$

For the PAL discussed in the paper, the back surface is chosen as a spherical surface with constant mean curvature. Therefore, from the formula (2.2), the progressive change for the optical power P of a PAL would be achieved by changing the mean curvature of the front surface smoothly and progressively. In this paper, the design objective is to determine the shape of the front surface of the PAL. For brevity, the optical power P is referred to as the power of the front surface in the remainder of the paper. The optical power is measured in diopter, which is defined as the inverse of focal length (i.e. mean curvature) multiplied by $(n - 1)$. Therefore, the diopter is of unit 1/meter.

The other crucial design parameter for PALs is called as the (surface) astigmatism or cylinder. Suppose κ_1 and κ_2 are the two local principal curvatures of the front surface, then the astigmatism of a lens is defined as

$$A = (n - 1)|\kappa_1 - \kappa_2|, \quad (2.3)$$

and the unit of astigmatism is also used as diopter. We can see that the two parameters of interest for a PAL design, optical power and astigmatism, are only related to the sum and the difference of the two principal curvatures, respectively. In general, the optical power is needed to provide the appropriate corrections for patients, while the astigmatism is an undesirable effect for a PAL design in the paper. Because if a lens has severe astigmatism, vision distortion will occur and the spectacle wearer will feel uncomfortable, unless the wearer has any astigmatic defect of their eyes.

An ideal PAL is one with the prescribed smooth progressive optical power distribution and with the zero astigmatism everywhere on the lens. However, in order to attain zero astigmatism on the whole surface, the surface must be a plane or a sphere, which cannot provide prescribed progressive power. Therefore, the two key design factors, of reaching the desired distribution of optical power and the undesired astigmatism, compete with each other. Following the above observation, Loos et al. proposed a method for determining the shapes of thin progressive lenses, which enables the designers to create a large variety of different designs. Based on their method, to design the surface of PALs, we can minimize the following functional [7]:

$$J(u) = \int_{\Omega} \left[\alpha(x, y) \left(\frac{\kappa_1 - \kappa_2}{2} \right)^2 + \beta(x, y) \left(\frac{\kappa_1 + \kappa_2}{2} - P_0(x, y) \right)^2 \right] dA, \quad (2.4)$$

where $\Omega \subset \mathbb{R}^2$ is a bounded domain, $u := u(x, y)$ defines the shape of the designed lens surface, $\kappa_1 := \kappa_1(x, y)$ and $\kappa_2 := \kappa_2(x, y)$ represent the two principal curvatures of the surface, respectively, dA represents the area element on the graph of $u(x, y)$, and the three functions $\alpha := \alpha(x, y)$, $\beta := \beta(x, y)$ and $P_0 := P_0(x, y)$ are previously prescribed functions in Ω . More precisely, the prescribed function P_0 is the desired distribution of optical power, and its magnitude increases continuously from the far-view region to the near-view region; the weight functions α and β control the ratio relation between the occurrence of astigmatism and the derivation from the prescribed power distribution function P_0 .

Substituting the mean curvature H and Gauss curvature K defined as

$$H := H(x, y) = \frac{\kappa_1 + \kappa_2}{2}, \quad (2.5)$$

$$K := K(x, y) = \kappa_1\kappa_2, \quad (x, y) \in \Omega,$$

into the functional (2.4), we can formulate the problem for designing PALs as the following minimization problem:

$$(\mathbf{P}) \text{ Min } J(u) = \int_{\Omega} [\alpha(x, y) (H^2(x, y) - K(x, y)) + \beta(x, y) (H(x, y) - P_0(x, y))^2] dA. \quad (2.6)$$

Suppose that in the Cartesian coordinates the surface of a lens is given by the graph function $z = u(x, y)$ for $(x, y) \in \Omega$, then the mean curvature H and Gauss curvature K can be given by

$$H = \frac{(1 + u_x^2)u_{yy} - 2u_xu_yu_{xy} + (1 + u_y^2)u_{xx}}{2g^3}, \quad (2.7)$$

$$K = \frac{u_{xx}u_{yy} - u_{xy}^2}{g^4},$$

and the area element dA can be expressed by

$$dA = g \, dx dy, \quad \text{with } g = \sqrt{1 + u_x^2 + u_y^2}, \quad (x, y) \in \Omega. \quad (2.8)$$

Plugging (2.7) and (2.8) into (2.6), we obtain the functional minimization problem for designing a PAL lens.

The Euler–Lagrange equation with respect to the functional in (2.6) is a highly nonlinear and high order partial differential equation. Therefore, it is generally very difficult and challenging to solve the problem (\mathbf{P}) by direct numerical computation. In the literatures, Wang et al. [11,9,12] adopted the linearization approximation method for the Euler–Lagrange equation generated from the variational problem (\mathbf{P}) to design PALs. By assuming that the designed lens surfaces are a combination of two parts (one is a prescribed spherical background surface and the other is a small perturbation surface with respect to the chosen spherical surface) they simplified the Euler–Lagrange equation with respect to the functional in (2.6) to a linear fourth-order partial differential equation. Under the various boundary conditions including clamped, partially clamped and natural boundary conditions, they showed the existence and uniqueness as well as the regularity of the solutions with respect to the linear fourth-order partial differential equation [11]. Furthermore, by using the B -spline finite element method, they designed a numerical algorithm for solving the linearized problem [9].

2.2. Linearization about the background surface

Following the linearization approach proposed by Wang et al. [11,9] for designing PALs, we assume that the surface function $u(x, y)$ can be divided into two parts:

$$u(x, y) = w(x, y) + v(x, y), \quad (x, y) \in \Omega, \quad (2.9)$$

where $w := w(x, y)$ is a chosen background surface and $v := v(x, y)$ represents the perturbation surface. Therefore, the functional minimization problem **(P)** with respect to $u(x, y)$ can be converted to the problem with respect to the small perturbation function $v(x, y)$. Substituting (2.9) into (2.7) and (2.8) and further assuming that the perturbation function $v(x, y)$ satisfies that $|\nabla v| \approx 0$ and $|\nabla^2 v|$ is bounded from above in the domain Ω , we can obtain the approximation expressions for H , K and g as

$$\begin{aligned} H &\approx \widehat{H}(v; w) \\ &= H(w) + \frac{(1 + w_x^2)v_{yy} - 2w_x w_y v_{xy} + (1 + w_y^2)v_{xx}}{2\widehat{g}^3}, \\ &(x, y) \in \Omega, \end{aligned} \quad (2.10)$$

$$\begin{aligned} K &\approx \widehat{K}(v; w) \\ &= \frac{(w_{xx} + v_{xx})(w_{yy} + v_{yy}) - (w_{xy} + v_{xy})^2}{\widehat{g}^4}, \end{aligned} \quad (2.11)$$

$$g \approx \widehat{g} = \sqrt{1 + w_x^2 + w_y^2}.$$

Inserting (2.10) and (2.11) into (2.6), we obtain the following functional which is an approximation to $J(u)$ in (2.6):

$$I(v; w) = \int_{\Omega} [(\alpha + \beta)\widehat{H}^2 - 2\beta P_0 \widehat{H} - \alpha \widehat{K} + \beta P_0^2] \widehat{g} \, dx dy. \quad (2.12)$$

For any given background surface $w(x, y)$, substituting (2.10) and (2.11) into (2.12), we can easily find that the functional $I(v; w)$ only depends on the second-order partial derivatives of the perturbation function $v(x, y)$, i.e. the terms v_{xx} , v_{xy} , v_{yy} , and they are all in quadratic form. It should be noted that, for simplicity, we can drop all the constant terms in expression (2.12) and still denote the functional as $I(v; w)$, then the functional $I(v; w)$ can be expressed by the following quadratic functional form:

$$I(v; w) = \int_{\Omega} \mathcal{F}(x, y, v_{xx}, v_{xy}, v_{yy}) \, dx dy, \quad (2.13)$$

where the integrand $\mathcal{F}(x, y, v_{xx}, v_{xy}, v_{yy})$ is continuous for all the arguments $x, y, v_{xx}, v_{xy}, v_{yy}$ and can be defined as

$$\begin{aligned} \mathcal{F}(x, y, v_{xx}, v_{xy}, v_{yy}) &= a_1 v_{xx}^2 + a_2 v_{xy}^2 + a_3 v_{yy}^2 + a_4 v_{xx} v_{yy} \\ &+ a_5 v_{xy} v_{yy} + a_6 v_{xx} v_{xy} + a_7 v_{xx} + a_8 v_{xy} + a_9 v_{yy}, \end{aligned} \quad (2.14)$$

where the coefficients a_i for $i = 1, 2, \dots, 9$ are given by

$$a_1 = \frac{(1 + w_y^2)^2}{4\widehat{g}^5}(\alpha + \beta), \quad a_2 = \frac{w_x^2 w_y^2}{\widehat{g}^5}(\alpha + \beta) + \frac{\alpha}{\widehat{g}^3},$$

$$a_3 = \frac{(1 + w_x^2)^2}{4\widehat{g}^5}(\alpha + \beta),$$

$$a_4 = \frac{(1 + w_x^2)(1 + w_y^2)}{2\widehat{g}^5}(\alpha + \beta) - \frac{\alpha}{\widehat{g}^3},$$

$$a_5 = -\frac{w_x w_y (1 + w_x^2)}{\widehat{g}^5}(\alpha + \beta),$$

$$a_6 = -\frac{w_x w_y (1 + w_y^2)}{\widehat{g}^5}(\alpha + \beta),$$

$$a_7 = \frac{(1 + w_y^2)H(w)}{\widehat{g}^2}(\alpha + \beta) - \frac{w_{yy}}{\widehat{g}^3}\alpha - \frac{1 + w_y^2}{\widehat{g}^2}\beta P_0,$$

$$a_8 = -\frac{2w_x w_y H(w)}{\widehat{g}^2}(\alpha + \beta) + \frac{2w_{xy}}{\widehat{g}^3}\alpha + \frac{2w_x w_y}{\widehat{g}^2}\beta P_0,$$

$$\begin{aligned} a_9 &= \frac{(1 + w_x^2)H(w)}{\widehat{g}^2}(\alpha + \beta) - \frac{w_{xx}}{\widehat{g}^3}\alpha \\ &- \frac{1 + w_x^2}{\widehat{g}^2}\beta P_0, \quad (x, y) \in \Omega. \end{aligned}$$

In the literature [11,9,12] and in this paper, for simplicity, the background surface is often chosen as spherical, i.e.

$$w(x, y) = \sqrt{R^2 - x^2 - y^2}, \quad (x, y) \in \Omega, \quad (2.15)$$

where R is a constant to be determined. Under the spherical background surface for w , noticing (2.7), we get

$$\begin{aligned} H(w) &= -\frac{1}{R}, \quad w_x = -\frac{x}{(R^2 - x^2 - y^2)^{1/2}}, \\ w_y &= -\frac{y}{(R^2 - x^2 - y^2)^{1/2}}, \quad (x, y) \in \Omega, \\ w_{xx} &= \frac{-R^2 + y^2}{(R^2 - x^2 - y^2)^{3/2}}, \quad w_{xy} = -\frac{xy}{(R^2 - x^2 - y^2)^{3/2}}, \\ w_{yy} &= \frac{-R^2 + x^2}{(R^2 - x^2 - y^2)^{3/2}}. \end{aligned}$$

We remark here that other kinds of background surfaces can also be used but we omit their investigation and discussion here for brevity.

Since the lenses in use are often circular, in practice, for designing a PAL lens, the computational domain Ω is usually chosen as a larger square containing the circular domain. When one finally finishes the design, one can ignore the other part and keep the targeted circular part as the prototype for manufacturing. Therefore, in our theoretical design, we always choose the computational domain as $\Omega = [-\frac{L}{2}, \frac{L}{2}]^2$ with L as the length of the square.

Since the functional (2.13) with (2.14) is a typical quadratic functional and it only depends on the second-order partial derivatives with respect to the perturbation function $v(x, y)$, thus if a function $v_0(x, y)$ minimizes the functional $I(v; w)$, then it is easy to check that the function $v_0(x, y) + l(x, y)$ also minimizes the functional $I(v; w)$ provided that $l(x, y)$ is a linear function on the domain Ω , i.e. $l(x, y) = c_1 x + c_2 y + c_3$ with c_1, c_2 and c_3 any three given constants. In order to ensure the uniqueness of the minimizer to the minimization problem, we might fix the values of the perturbation surface $v(x, y)$ at three points, e.g. three corners, of the domain Ω . Therefore, for designing the surface of PALs, we need to solve the following linearized functional minimization problem with respect to the perturbation surface function $v := v(x, y)$:

$$\text{(LP)} \begin{cases} \text{Min } I(v; w) = \int_{\Omega = [-\frac{L}{2}, \frac{L}{2}]^2} \mathcal{F}(x, y, v_{xx}, v_{xy}, v_{yy}) \, dx dy, \\ v\left(-\frac{L}{2}, -\frac{L}{2}\right) = v\left(-\frac{L}{2}, \frac{L}{2}\right) = v\left(\frac{L}{2}, \frac{L}{2}\right) = 0, \end{cases} \quad (2.16)$$

where the background surface w is chosen as a spherical surface as (2.15).

3. Numerical algorithm

In the section, we will present a variational-difference numerical method for solving the linearized functional minimization problem **(LP)** by approximating the integral via trapezoid quadrature rule and derivatives via finite differences.

Denote the mesh size $h = \Delta x = \Delta y := \frac{L}{N}$ with N a given positive integers and define

$$x_i = -\frac{L}{2} + ih, \quad i = 0, 1, \dots, N;$$

$$y_j = -\frac{L}{2} + jh, \quad j = 0, 1, \dots, N.$$

We partition the domain Ω into N^2 sub-squares as $\Omega_{ij} = \{(x, y) \mid x_i \leq x \leq x_{i+1}, y_j \leq y \leq y_{j+1}\}$ for $i, j = 0, 1, \dots, N - 1$.

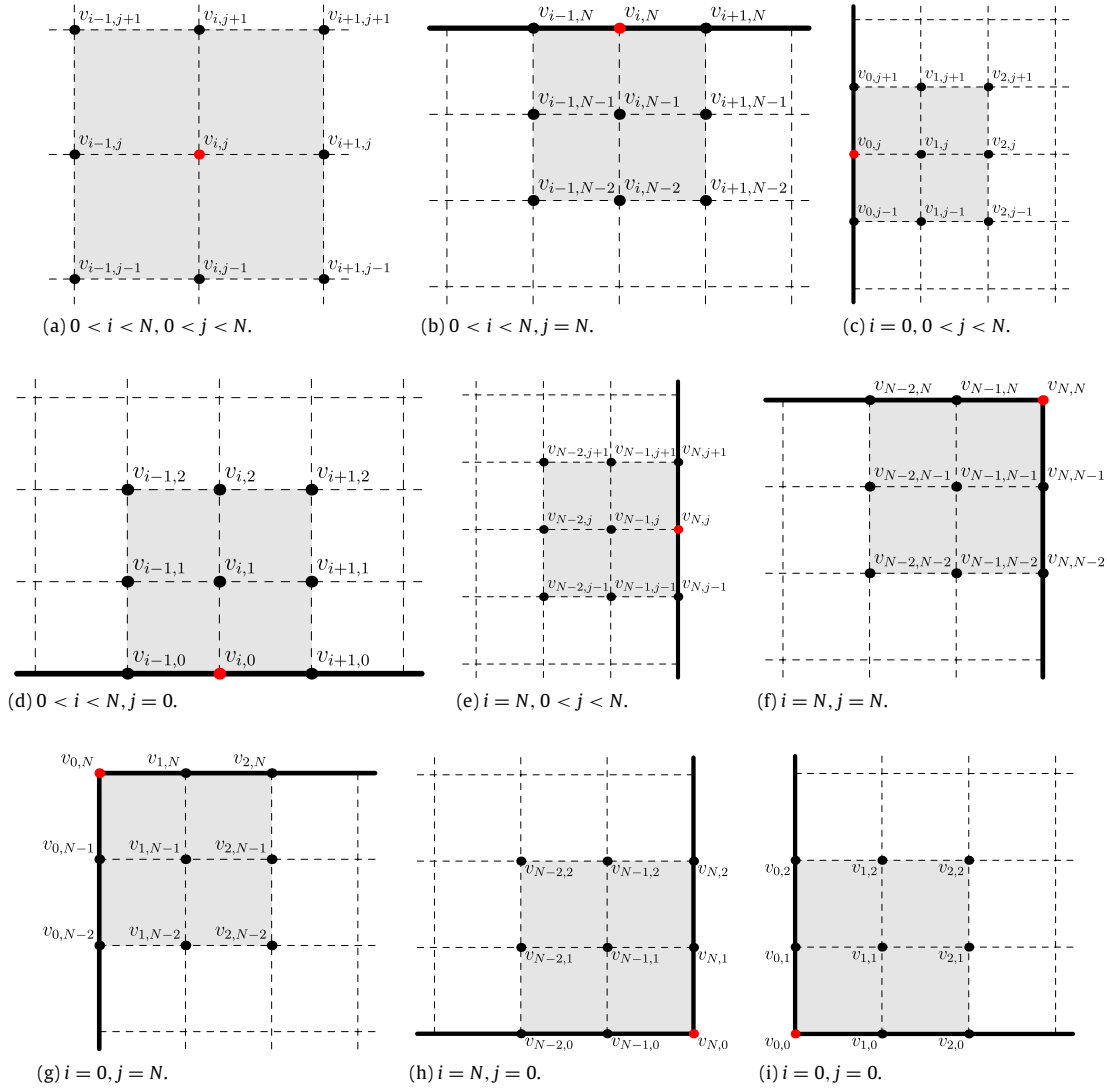


Fig. 2. A schematic illustration of the stencils used to approximate the second-order partial derivatives v_{xx} , v_{xy} and v_{yy} at the grid point (x_i, y_j) (labeled as the red point) under nine different cases, (a)–(e) when $(x_i, y_j) \in \mathcal{R}_h$; (b)–(e) when $(x_i, y_j) \in \mathcal{S}_h^1$; and (f)–(i) when $(x_i, y_j) \in \mathcal{S}^0$. (For interpretation of the references to colour in this figure legend, the reader is referred to the web version of this article.)

Denote \mathcal{T}_h as the set of all grid points, i.e. $\mathcal{T}_h = \{(x_i, y_j) \mid i, j = 0, 1, \dots, N\}$, which is divided into the set of grid points inside Ω , i.e. $\mathcal{R}_h = \{(x_i, y_j) \mid i, j = 1, 2, \dots, N - 1\}$, and the set of grid points on the boundary of Ω , i.e. $\mathcal{S}_h = \{(x_i, y_0) \text{ or } (x_i, y_N) \mid i = 0, 1, \dots, N\} \cup \{(x_0, y_j) \text{ or } (x_N, y_j) \mid j = 0, 1, \dots, N\}$. In addition, \mathcal{S}_h is further split into the set of corner points, i.e. $\mathcal{S}^0 = \{(x_0, y_0), (x_0, y_N), (x_N, y_0), (x_N, y_N)\}$, and the set of the remaining points on the boundary, i.e. $\mathcal{S}_h^1 = \{(x_i, y_0) \text{ or } (x_i, y_N) \mid i = 1, 2, \dots, N - 1\} \cup \{(x_0, y_j) \text{ or } (x_N, y_j) \mid j = 1, 2, \dots, N - 1\}$. Thus we have $\mathcal{T}_h = \mathcal{R}_h \cup \mathcal{S}_h = \mathcal{R}_h \cup \mathcal{S}_h^1 \cup \mathcal{S}^0$ and $\mathcal{S}_h = \mathcal{S}_h^1 \cup \mathcal{S}^0$. Based on this partition, we can approximate the integral in (2.16) via the composite trapezoid rule as

$$\begin{aligned}
 I(v; w) &= \sum_{i=0}^{N-1} \sum_{j=0}^{N-1} \int_{\Omega_{ij}} \mathcal{F}(x, y, v_{xx}, v_{xy}, v_{yy}) \, dx dy \\
 &\approx \sum_{i=0}^{N-1} \sum_{j=0}^{N-1} \frac{h^2}{4} (\mathcal{F}_{i,j} + \mathcal{F}_{i,j+1} + \mathcal{F}_{i+1,j} + \mathcal{F}_{i+1,j+1}) \\
 &= h^2 \left[\sum_{(x_i, y_j) \in \mathcal{R}_h} \mathcal{F}_{i,j} + \frac{1}{2} \sum_{(x_i, y_j) \in \mathcal{S}_h^1} \mathcal{F}_{i,j} \right.
 \end{aligned}$$

$$\left. + \frac{1}{4} \sum_{(x_i, y_j) \in \mathcal{S}^0} \mathcal{F}_{i,j} \right], \tag{3.1}$$

where

$$\mathcal{F}_{i,j} = \mathcal{F}(x_i, y_j, v_{xx}(x_i, y_j), v_{xy}(x_i, y_j), v_{yy}(x_i, y_j)), \tag{3.2}$$

$i, j = 0, 1, \dots, N.$

In order to further discretize (3.1), we approximate the derivatives in (3.2) via finite differences. Let $v_{i,j}$ be the numerical approximation of $v(x_i, y_j)$ for $i, j = 0, 1, \dots, N$ and denote the vector $\mathbf{V} = \{v_{i,j} \mid i, j = 0, 1, \dots, N\}$. Introduce the following standard finite difference operators (see Fig. 2(a)–(i)):

$$\delta_x^2 v_{i,j} = \frac{1}{h^2} \begin{cases} v_{i-1,j} - 2v_{i,j} + v_{i+1,j}, & i = 1, 2, \dots, N - 1, \\ v_{0,j} - 2v_{1,j} + v_{2,j}, & i = 0, \\ v_{N,j} - 2v_{N-1,j} + v_{N-2,j}, & i = N, \end{cases} \tag{3.3}$$

$j = 0, 1, \dots, N,$

$$\delta_y^2 v_{i,j} = \frac{1}{h^2} \begin{cases} v_{i,j-1} - 2v_{i,j} + v_{i,j+1}, & j = 1, 2, \dots, N - 1, \\ v_{i,0} - 2v_{i,1} + v_{i,2}, & j = 0, \\ v_{i,N} - 2v_{i,N-1} + v_{i,N-2}, & j = N, \end{cases} \tag{3.4}$$

$i = 0, 1, \dots, N,$

$$\delta_{xy}v_{i,j} = \frac{1}{4h^2} \begin{cases} v_{i-1,j-1} - v_{i-1,j+1} - v_{i+1,j-1} + v_{i+1,j+1}, \\ i, j = 1, 2, \dots, N-1, \\ v_{0,j-1} - v_{0,j+1} - v_{2,j-1} + v_{2,j+1}, \\ i = 0, j = 1, 2, \dots, N-1, \\ v_{N-2,j-1} - v_{N-2,j+1} - v_{N,j-1} + v_{N,j+1}, \\ i = N, j = 1, 2, \dots, N-1, \\ v_{i-1,0} - v_{i-1,2} - v_{i+1,0} + v_{i+1,2}, \\ j = 0, i = 1, 2, \dots, N-1, \\ v_{i-1,N-2} - v_{i-1,N} - v_{i+1,N-2} + v_{i+1,N}, \\ j = N, i = 1, 2, \dots, N-1, \\ v_{0,0} - v_{0,2} - v_{2,0} + v_{2,2}, \\ i = 0, j = 0, \\ v_{0,N-2} - v_{0,N} - v_{2,N-2} + v_{2,N}, \\ i = 0, j = N, \\ v_{N-2,0} - v_{N-2,2} - v_{N,0} + v_{N,2}, \\ i = N, j = 0, \\ v_{N-2,N-2} - v_{N-2,N} - v_{N,N-2} + v_{N,N}, \\ i = N, j = N. \end{cases} \quad (3.5)$$

Then the second-order derivatives at the grid points can be approximated as

$$v_{xx}(x_i, y_j) = \delta_x^2 v_{i,j} + \begin{cases} O(h^2), & (x_i, y_j) \in \mathcal{R}_h, \\ O(h), & (x_i, y_j) \in \mathcal{S}_h, \end{cases} \approx \delta_x^2 v_{i,j}, \quad (3.6)$$

$$v_{yy}(x_i, y_j) = \delta_y^2 v_{i,j} + \begin{cases} O(h^2), & (x_i, y_j) \in \mathcal{R}_h, \\ O(h), & (x_i, y_j) \in \mathcal{S}_h, \end{cases} \approx \delta_y^2 v_{i,j}, \quad (3.7)$$

$i, j = 0, 1, \dots, N,$

$$v_{xy}(x_i, y_j) = \delta_{xy} v_{i,j} + \begin{cases} O(h^2), & (x_i, y_j) \in \mathcal{R}_h, \\ O(h), & (x_i, y_j) \in \mathcal{S}_h, \end{cases} \approx \delta_{xy} v_{i,j}. \quad (3.8)$$

Plugging (3.6)–(3.8) into (3.1), we obtain an approximation to the functional $I(v; w)$ as

$$I(v; w) \approx h^2 \left[\sum_{(x_i, y_j) \in \mathcal{R}_h} \mathcal{F}_{i,j}^h + \frac{1}{2} \sum_{(x_i, y_j) \in \mathcal{S}_h^1} \mathcal{F}_{i,j}^h + \frac{1}{4} \sum_{(x_i, y_j) \in \mathcal{S}^0} \mathcal{F}_{i,j}^h \right] := I_h(\mathbf{V}), \quad (3.9)$$

where

$$\mathcal{F}_{i,j}^h = \mathcal{F}(x_i, y_j, \delta_x^2 v_{i,j}, \delta_{xy} v_{i,j}, \delta_y^2 v_{i,j}), \quad i, j = 0, 1, \dots, N. \quad (3.10)$$

Thus the linearized functional minimization problem (2.16) can be approximated by the following finite-dimensional minimization problem:

$$(\mathbf{LP}^h) \begin{cases} \mathbf{Min} I_h(\mathbf{V}) = h^2 \left[\sum_{(x_i, y_j) \in \mathcal{R}_h} \mathcal{F}_{i,j}^h + \frac{1}{2} \sum_{(x_i, y_j) \in \mathcal{S}_h^1} \mathcal{F}_{i,j}^h + \frac{1}{4} \sum_{(x_i, y_j) \in \mathcal{S}^0} \mathcal{F}_{i,j}^h \right], \\ \mathbf{V} \in \mathbb{R}^{(N+1)^2} \text{ satisfying } v_{0,0} = v_{0,N} = v_{N,N} = 0. \end{cases} \quad (3.11)$$

Since the functional $I_h(\mathbf{V})$ is a quadratic form of the vector \mathbf{V} , thus the minimization problem (3.11) admits a minimizer which is also a solution of the following linear system:

$$\frac{\partial I_h(\mathbf{V})}{\partial v_{i,j}} = 0, \quad i, j = 0, 1, \dots, N. \quad (3.12)$$

Inserting the constraints $v_{0,0} = v_{0,N} = v_{N,N} = 0$ into the linear system (3.12), we obtain a linear system with $(N+1)^2 - 3$ unknowns for finding the vector \mathbf{V} , whose coefficient matrix is sparse and symmetric, thus it can be solved very efficiently. We remark here that, if the perturbation surface v is smooth, then

the above discretization is the second-order approximation for the linearized functional. In fact, by denoting

$$I_h(v; w) := h^2 \left[\sum_{(x_i, y_j) \in \mathcal{R}_h} \hat{\mathcal{F}}_{i,j}^h + \frac{1}{2} \sum_{(x_i, y_j) \in \mathcal{S}_h^1} \hat{\mathcal{F}}_{i,j}^h + \frac{1}{4} \sum_{(x_i, y_j) \in \mathcal{S}^0} \hat{\mathcal{F}}_{i,j}^h \right], \quad (3.13)$$

with

$$\hat{\mathcal{F}}_{i,j}^h = \mathcal{F}(x_i, y_j, \delta_x^2 v(x_i, y_j), \delta_{xy} v(x_i, y_j), \delta_y^2 v(x_i, y_j)), \quad i, j = 0, 1, \dots, N, \quad (3.14)$$

noticing (3.1), (2.14), (3.2) and (3.6)–(3.8), using the triangle inequality, we have

$$\begin{aligned} |I(v; w) - I_h(v; w)| &\leq \sum_{i=0}^{N-1} \sum_{j=0}^{N-1} \left| \int_{\Omega_{ij}} \mathcal{F}(x, y, v_{xx}, v_{xy}, v_{yy}) dx dy \right. \\ &\quad \left. - \frac{h^2}{4} (\mathcal{F}_{i,j} + \mathcal{F}_{i,j+1} + \mathcal{F}_{i+1,j} + \mathcal{F}_{i+1,j+1}) \right| \\ &\quad + h^2 \left[\sum_{(x_i, y_j) \in \mathcal{R}_h} |\mathcal{F}_{i,j} - \hat{\mathcal{F}}_{i,j}^h| + \frac{1}{2} \sum_{(x_i, y_j) \in \mathcal{S}_h^1} |\mathcal{F}_{i,j} - \hat{\mathcal{F}}_{i,j}^h| \right. \\ &\quad \left. + \frac{1}{4} \sum_{(x_i, y_j) \in \mathcal{S}^0} |\mathcal{F}_{i,j} - \hat{\mathcal{F}}_{i,j}^h| \right] \\ &\leq \sum_{i=0}^{N-1} \sum_{j=0}^{N-1} C_1 h^4 + h^2 \left[\sum_{(x_i, y_j) \in \mathcal{R}_h} C_2 h^2 \right. \\ &\quad \left. + \frac{1}{2} \sum_{(x_i, y_j) \in \mathcal{S}_h^1} C_3 h + \frac{1}{4} \sum_{(x_i, y_j) \in \mathcal{S}^0} C_4 h \right] \\ &\leq C_1 h^4 N^2 + h^2 [C_2 h^2 (N-1)^2 + 2C_3 h (N-1) + C_4 h] \\ &\leq Ch^2, \end{aligned} \quad (3.15)$$

where C_1, C_2, C_3, C_4 and C are positive constants depending on the function v and the coefficients a_i in (2.14), but they are independent of the mesh size h . We assume here that the integrand function $\mathcal{F}(x, y, v_{xx}, v_{xy}, v_{yy})$ is C^2 -continuous for $(x, y) \in \Omega$.

4. Results and discussion

In this section, we present several simulation results using the variational-difference method proposed above to demonstrate its high performance. Because in practice PALs are often designed on a circular region with the diameter of about 80 mm, we use the computational domain $\Omega = [-40, 40]^2$ containing the circular domain with the length unit mm. The grid numbers N along the x and y directions were chosen to be 80 except where noted. The convergence was checked by continuously reducing the grid sizes. The computational time for each simulation under the grid number $N = 80$ was several seconds on a laptop with a CPU Intel Core i5-3317U 1.7 GHz. For all simulations presented in the paper, we chose the refractive index $n = 1.53$.

We discuss how to assign the three previously given functions involved in the design functional: the weight functions $\alpha(x, y)$, $\beta(x, y)$, and the prescribed optical power (i.e. mean curvature) distribution $P_0(x, y)$. Following the procedure used by Loos et al. [7] and Wang et al. [9], we can divide the computational

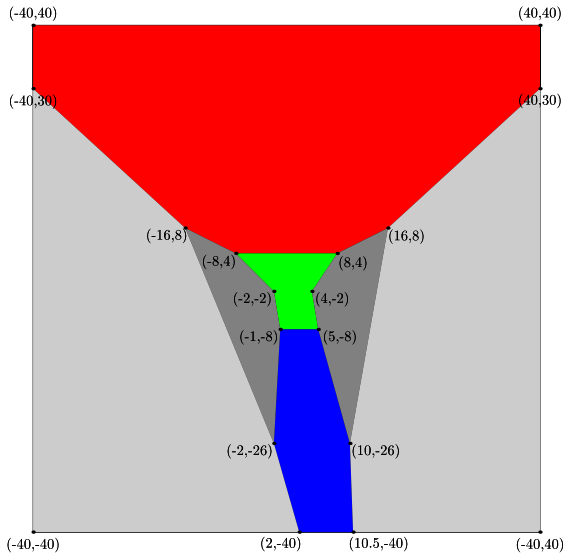


Fig. 3. A partition of seven subregions of the computational domain Ω . (For interpretation of the references to colour in this figure legend, the reader is referred to the web version of this article.)

Table 1

The PAL designs under two different patient's prescriptions (unit: diopter, 1/m).

Cases	Myopia	Presbyopia	PAL Prescription (BASE)	PAL Prescription (ADD)	Back surface
A	-2.00	2.00	5.00	2.00	7.00
B	-1.50	2.00	3.00	2.00	4.50

square domain Ω into seven subregions. Fig. 3 shows an example of the partition of seven subregions in Ω . As shown in Fig. 3, the large red subregion is used for distance-view, the small blue subregion is used for near-view, and the green subregion connecting the two is used for intermediate-view. The rest of the subregions in Ω belong to the blending zones, and we divide them into four in order to easily assign them the values of the weight functions and the prescribed mean curvature function.

First, we discuss how to assign the weight functions $\alpha(x, y)$ and $\beta(x, y)$. Based on the importance of the subregion to the PAL design, we assign a constant value to each subregion for the weight functions $\alpha(x, y)$ and $\beta(x, y)$. In a progressive lens design, the values of weight functions $\alpha(x, y)$ and $\beta(x, y)$ should be weighted the most in the distance-view, near-view and intermediate-view subregions. Therefore, we put more weight in these subregions and less weight in the other four blending subregions. Meanwhile, because the practically used domain of the progressive lens design is a circular domain centered at the origin of Ω with a radius of 30 mm (denoted as the domain \mathcal{D}), if a point belongs to the above seven subregions but is outside the domain \mathcal{D} , we forcefully put the least weight on it. On the other hand, we noticed that the smoothness of the solution depends on that of $\alpha(x, y)$, $\beta(x, y)$ and $P_0(x, y)$ in the simulations. Therefore, we used the convolution or average methods to smooth these discrete data. Fig. 4 shows the surface plots about the weight functions $\alpha(x, y)$ and $\beta(x, y)$ used in the simulations of the paper.

The assignment of the optical power (or mean curvature) distribution $P_0(x, y)$ must rely on every spectacle wearer's individual prescription. In general, there are two parameters for the power distribution: BASE power and ADD power. The BASE power is often defined as the power of the far-view region, and the ADD power is defined as the difference between the far-view and near-view regions. So the power of the near-view region is BASE+ADD. The BASE power and ADD power both have the unit of diopter. To remedy a patient who suffers from both presbyopia

Table 2

L_2 norm of the error and convergence rate for the perturbation function $v(x, y)$ under the two cases with different grid numbers. The numerical results were obtained under the spherical background surfaces with the radii of $R = 90$ mm for Case A and $R = 137$ mm for Case B.

Grid numbers	Case A	Convergence rate	Case B	Convergence rate
(80, 80)–(160, 160)	5.551e-02		5.033e-02	
(160, 160)–(320, 320)	1.384e-02	2.004	1.245e-02	2.015
(320, 320)–(640, 640)	3.520e-03	1.976	3.147e-03	1.984
(640, 640)–(1280, 1280)	8.853e-04	1.991	7.939e-04	1.987

and myopia, the PAL should be a relevant combination of the front and back surfaces. For example, if a patient suffers from myopia with -2.00 diopter and presbyopia with 2.00 diopter, a PAL may be designed with a combination of the back surface with 7.00 diopter and the front surface with 5.00 diopter BASE and 2.00 diopter ADD. The combination criterion is that ADD power must be equal to the presbyopia, and BASE power can be determined by the myopia and the back spherical surface power. We performed numerical simulations of two kinds of prescriptions for designing the free-form front surface of a PAL (shown by Table 1). Taking Case A for example, we assigned the mean curvature with unit of $1/\text{mm}$ of the far-view region (the red region shown in Fig. 3) as $-\frac{\text{BASE}}{1000(n-1)} = -0.00943$ (note that a spherical surface was assumed here to have a negative mean curvature); the mean curvature of the near-view region (the blue region shown in Fig. 3) was given as $-\frac{\text{BASE}+\text{ADD}}{1000(n-1)} = -0.0132$; a smooth function was assigned to connect with the above two parts in the green region shown in Fig. 3, and the mean curvatures of the other four regions were assigned as the average of the mean curvatures of the far-view and near-view regions. Then a smooth method was applied to smooth these discrete data. Fig. 5 is the prescribed mean curvature distribution $P_0(x, y)$ for Case A and Case B used in the simulations of the paper.

To check the accuracy and convergence rate of the proposed variational-difference method, we performed various numerical simulations for the linearized functional minimization problem (LP) under different grid numbers. Table 2 shows the L_2 norm of the error and convergence rate for the perturbation function $v(x, y)$ under the two cases with the grid numbers $N = 80, 160, 320, 640$ and 1280 . The numerical results were obtained under the spherical background surfaces with the radii of $R = 90$ mm for Case A and $R = 137$ mm for Case B, and the controlled parameters $\alpha(x, y)$, $\beta(x, y)$ and $P_0(x, y)$ involved in the computations were as presented above. The L_2 norm of the error was calculated by the following expression:

$$E_N = \left[\sum_{i=0}^{N-1} \sum_{j=0}^{N-1} [\mathbf{v}_{i,j}^N - \mathbf{v}_{2i,2j}^{2N}]^2 h^2 \right]^{1/2}, \quad (4.1)$$

where \mathbf{V}^N and \mathbf{V}^{2N} are the numerical solutions of (LP^h) (3.11) with $N + 1$ and $2N + 1$ grid points in each direction, respectively, and the convergence rate was calculated by $\log_2(E_N/E_{2N})$. The numerical results shown by Table 2 indicate that the convergence rate for the perturbation function $v(x, y)$ is of second-order accuracy in the sense of the L_2 norm. Compared with the B-spline finite element method [9], although the accuracy is almost the same, the memory usage and computational cost for our proposed method are smaller, because there is no need to compute the numerical quadrature at each element and it is much easier to assemble the stiffness matrix. The biggest advantage of the proposed variational-difference approach is that it is more straightforward and its computational process is much easier.

For the simulations, there is another important issue—how to choose the optimal radius R of spherical background surfaces. For each value of R , we can solve the corresponding quadratic

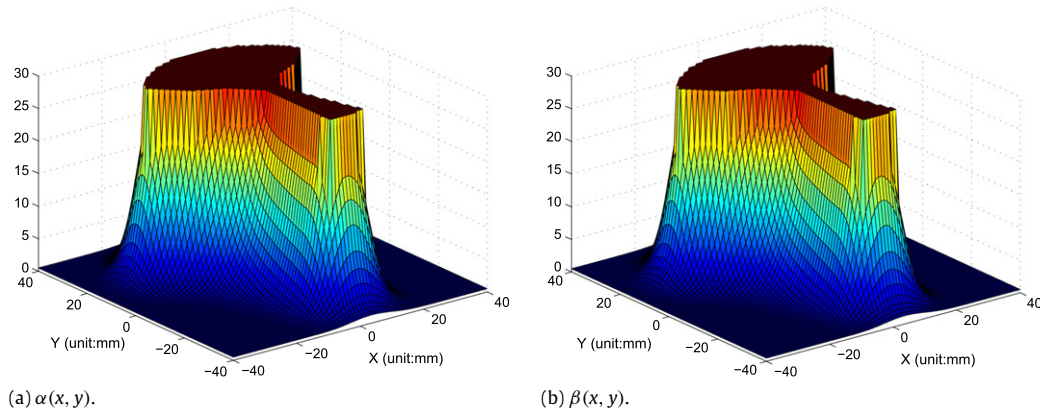


Fig. 4. Surface plots about the weight functions $\alpha(x, y)$ and $\beta(x, y)$.

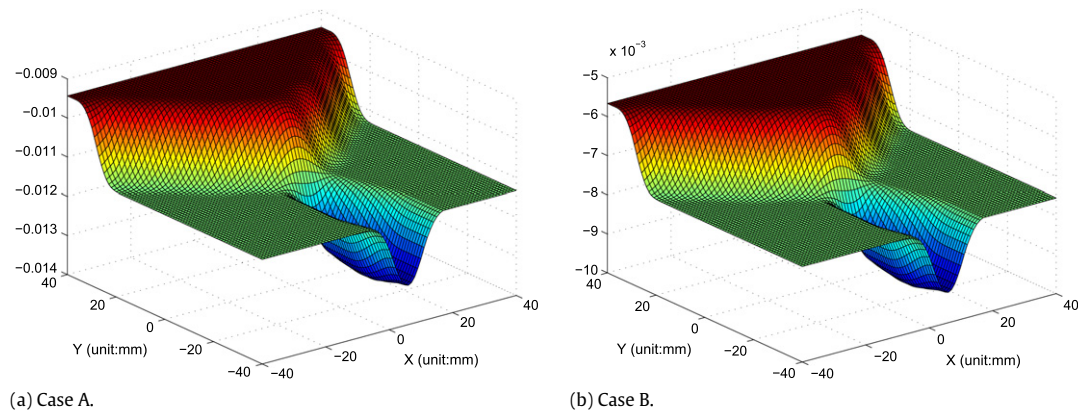


Fig. 5. Surface plots about the prescribed mean curvature distribution $P_0(x, y)$ for the two cases shown in Table 1, unit: 1/mm.

functional minimization problem (LP) in (2.16) to get the solution $v_R(x, y)$. Fig. 6 shows the numerical results for the perturbation surface $v_R(x, y)$ with respect to the four different radii of spherical background surfaces $R = 106, 98, 90, 80$ under Case A. As shown in Fig. 6, when the radius reduces from 106 mm to 80 mm, the shape of computed perturbation surface $v_R(x, y)$ gradually changes from hump to valley structures (similar behavior of the shape change as R decreases can be also observed under Case B, not shown here). We note that the shapes of $v_R(x, y)$, when $R = 106$ mm and $R = 98$ mm (shown by Fig. 6(a)–(b)), are very similar to the numerical result produced by Wang et al. in [9] using the B -spline finite element method under the natural boundary condition, which shows that the two methods produce almost the same numerical results. When we have the solution of $v_R(x, y)$, the designed surface of PAL can be given by $u_R(x, y) = v_R(x, y) + \sqrt{R^2 - x^2 - y^2}$. By this definition of u_R , we can define a weight function I_{disc} to determine the optimal spherical background surface:

$$I_{\text{disc}} = \int_{\mathcal{D}} [\alpha(x, y) (H_R^2(x, y) - K_R(x, y)) + \beta(x, y) (H_R(x, y) - P_0(x, y))^2] dA, \quad (4.2)$$

where the mean curvature H_R and Gauss curvature K_R are calculated by the solution of u_R , and \mathcal{D} is chosen as a circular domain centered at the origin of Ω with the radius of 30 mm. It should be noted that, since the produced solution by the variational-difference method is the values on the discrete points, in order to calculate the first and second derivatives with regard to computing the quantities such as curvatures, power and

astigmatism, we made use of these computed discrete values and fitted them as a smooth surface by tensor product B -splines of degree 5, and then calculated the derivatives on the interpolated surfaces. Fig. 7 shows the weight function I_{disc} as a function of the radius R under Case A and Case B. From the figure, we can clearly observe that there exists a critical value R_c at which the weight function I_{disc} attains the minimal value. In the following simulations, we chose the radii of spherical background surfaces as the optimal radius R_c given by Fig. 7. For Case A, the optimal radius R_c is equal to 90 mm; and for Case B, it is 137 mm.

By using the above optimal radius for the spherical background surface, we presented the numerical results for the surface of designed PALs under Case A and Case B shown by Figs. 8–10. Fig. 8 gives surface plots for the finally designed PAL surfaces under the two cases, and the designed surfaces are respectively very close to a spherical surface, which is consistent with the assumption in the paper. Figs. 9 and 10 both show the distribution for the power and astigmatism functions under the two cases, which are calculated by using the computed surfaces of PAL. The middle dashed circle in Fig. 9 gives the circular domain of radius smaller than 30 mm, i.e. \mathcal{D} mentioned above, which is the area practically used for a spectacle lens. As shown by Figs. 9 and 10, we can clearly see that the required ADD power of 2.0 diopter is reached for both the two cases, the power function changes progressively and smoothly, and also there is a clear “corridor” which connects with the far-view and near-view regions. On the other hand, the astigmatism also changes smoothly and the maximum astigmatism gets effectively controlled within less than 1.6 diopter, which is smaller than the prescribed ADD power of 2.0

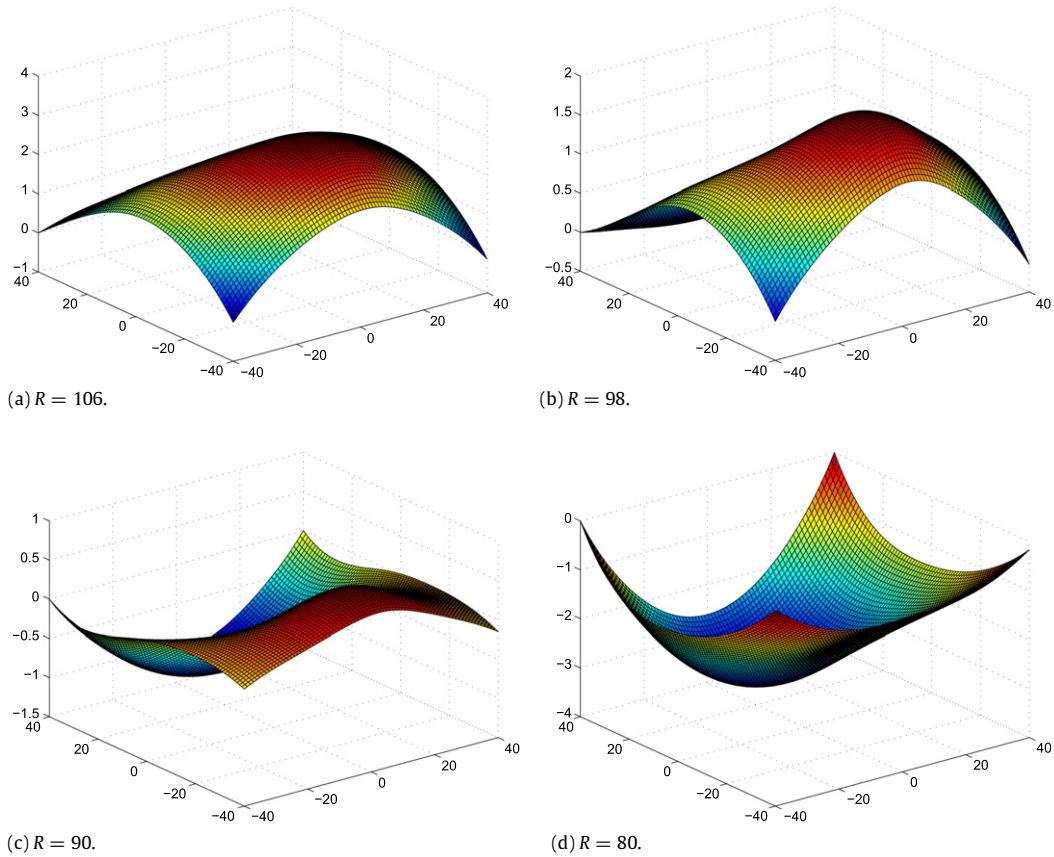


Fig. 6. Numerical results for the perturbation surface $v_R(x, y)$ with respect to four different spherical background surfaces under Case A, unit: mm.

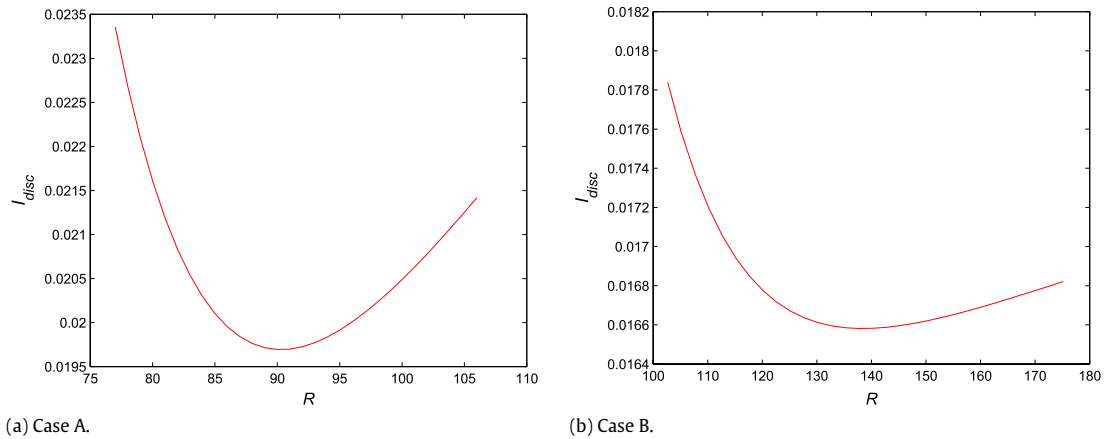


Fig. 7. The weight function I_{disc} as a function of the radius of spherical background surface R for the two cases.

diopter. These designs are better than typical PAL designs, which generally have the same maximum astigmatism and ADD power. The above numerical results demonstrated the efficiency and high performance as well as the simplicity for implementation of our proposed method.

5. Conclusions

In the paper, we have proposed a variational-difference method for designing the optical free form surface of PAL. The PAL, which has a front surface with three important zones including the far-view, near-view and intermediate zones, is often used to

remedy presbyopia by distributing optical powers of the three zones progressively and smoothly. Based on the controls between the refractive optical power deviating from the prescribed power distribution and the unwanted astigmatism, a functional minimization mathematical model was presented. By assuming that the front surface of PALs is a perturbed one around a spherical background surface, we linearized and simplified the mathematical model to a quadratical functional minimization problem. A variational-difference numerical method was proposed for solving the quadratical functional minimization problem. Compared with the existing literature which solves the problem by the *B*-spline finite element method, the essence of the proposed variational-difference numerical method lies in minimizing the

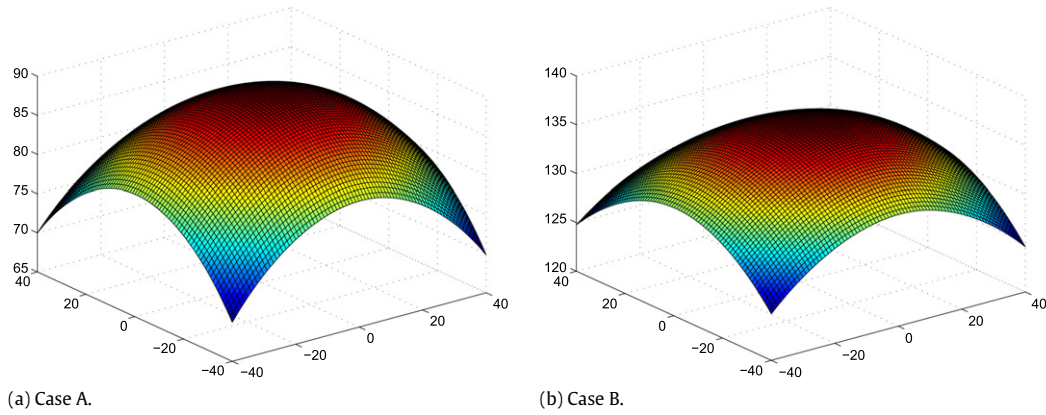


Fig. 8. Surface plots for the numerical results of designed PAL surfaces under the two cases, unit: mm.

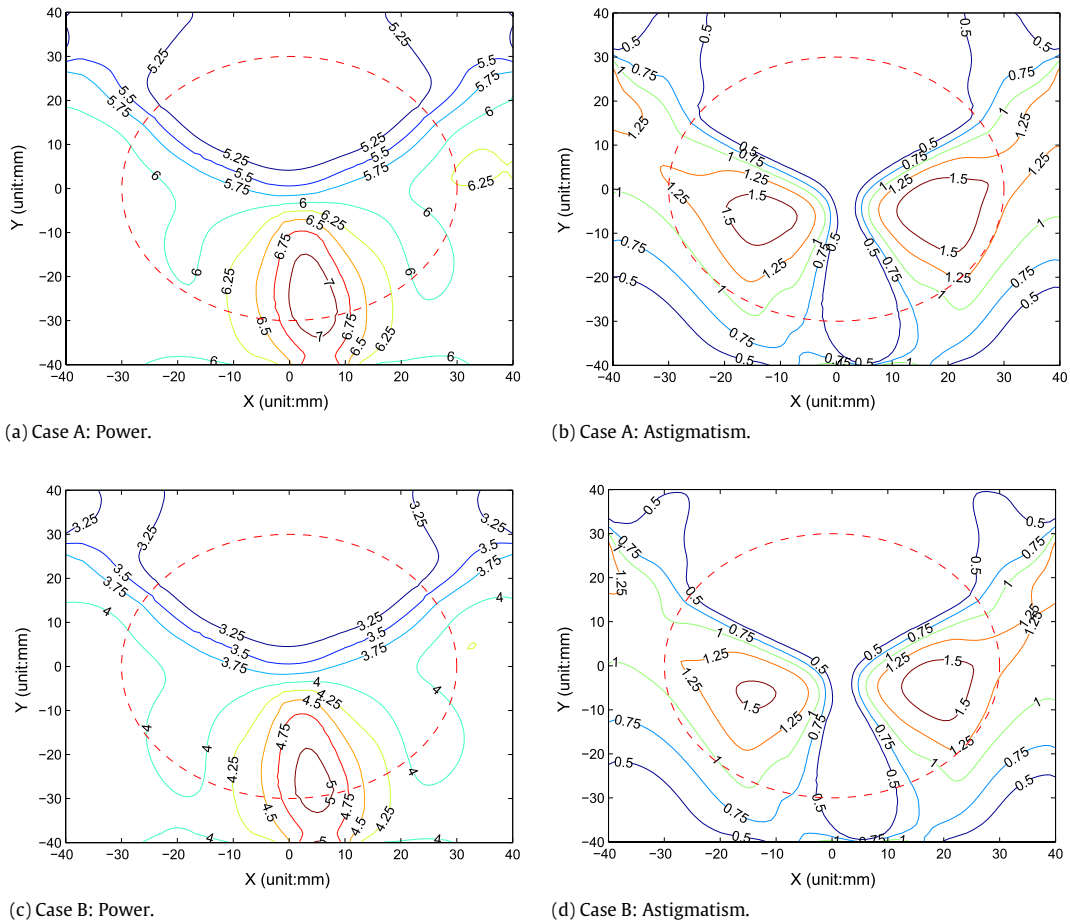


Fig. 9. Contour plots for the power and astigmatism distributions under the two cases, unit: diopter.

functional directly by the finite difference method rather than in approximating the solution of the corresponding Euler–Lagrange equation to the functional. It is very easily understood and implemented by optical engineers, and its memory and computational cost are smaller than that of the *B*-spline finite element method. Our extensive numerical results indicate that it can produce satisfactory designs for optical engineers in several seconds. We believe that our method could be a powerful candidate tool for designing various specifications of PALs.

In the present model, we used the perturbed background surface as a spherical surface and linearized the functional minimization problem (P) in (2.6) to a quadratic functional minimization problem (LP) in (2.16). So are there any better background sur-

faces, under which we might linearize the problem and obtain better design results? Future extensions may include the revolution surface and other surfaces as the background surfaces. On the other hand, we assumed that the back surface of the PAL is spherical in the paper and discussed how to design the free-form front surface. As a matter of fact, the coupling of the appropriately constructed design for both the back and front surfaces may produce more powerful and effective PALs, and this will be the trend for the design of new generation customized PALs. In future work, we will consider the design of both the back and front surfaces simultaneously, and incorporate more complicated design objectives, such as prescribed astigmatism, prism and many others, into the models.

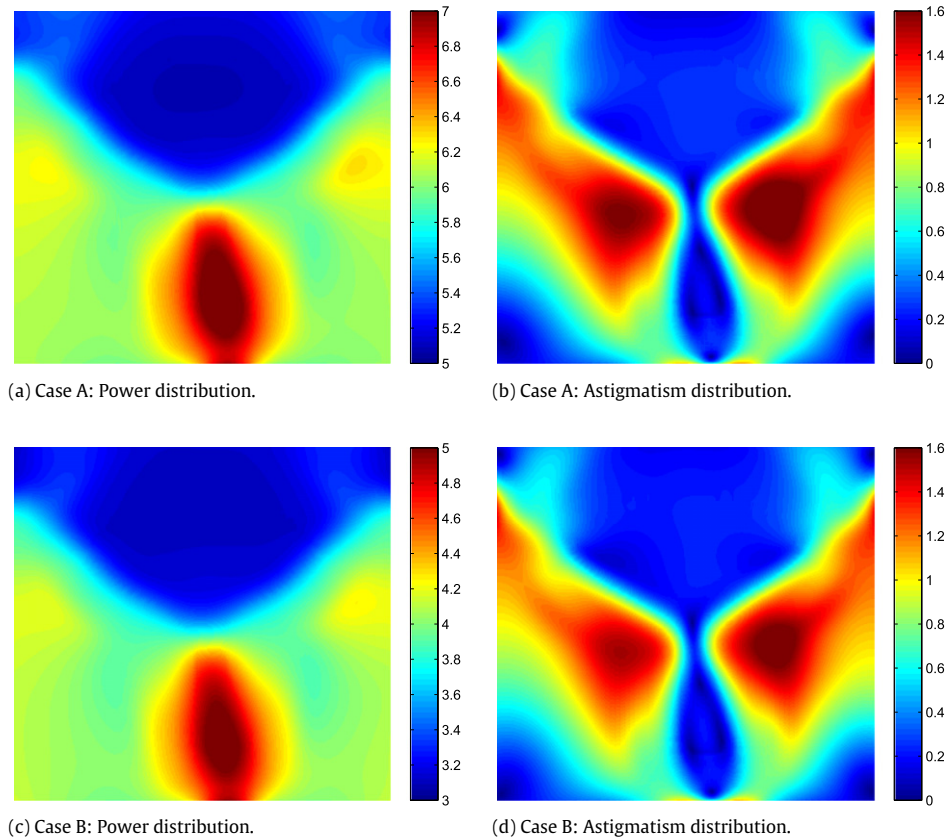


Fig. 10. Numerical results about the power and astigmatism distributions under the two cases, unit: diopter.

Acknowledgments

The authors would like to express their sincere thanks to Dr. Xiangdong Liu (Delta Optics Technologies Pte Ltd., Singapore) for introducing the problem to them. This work is partially supported by the Singapore A*STAR SERC PSF-Grant No. 1321202067 (W. Bao and Q. Tang), and the National Natural Science Foundation of China under Grant No. 11261065 (H. Wang).

References

- [1] Aves O. Improvements in and relating to multifocal lenses and the like, and the method of grinding same. GB Patent 1908. 15735.
- [2] Meister DJ, Fisher SW. Progress in the spectacle correction of presbyopia, part I: design and development of progressive lenses. *Clin Exp Optom* 2008;91: 240–50.
- [3] Meister DJ, Fisher SW. Progress in the spectacle correction of presbyopia, part II: modern progressive lens technologies. *Clin Exp Optom* 2008;91:251–64.
- [4] Winthrop JT. Progressive addition spectacle lens. US Patent 1989. 4861153.
- [5] Winthrop JT. Progressive addition spectacle lens. US Patent 1992. 313689.
- [6] Baudart T, Ahsbahs F, Miede C. Multifocal ophthalmic lens. US Patent 2000. 6102544.
- [7] Loos J, Greiner G, Seidel HP. A variational approach to progressive lens design. *Comput Aided Des* 1998;30:595–602.
- [8] Loos J, Slusallek P, Seidel HP. Using wavefront tracing for visualization and optimization of progressive lenses. In: *EUROGRAPHICS*, Vol. 17, 1998. p. 255–65.
- [9] Wang J, Santosa F. A numerical method for progressive lens design. *Math Models Methods Appl Sci* 2004;14:619–40.
- [10] Hsu WY, Liu YL, Cheng YC, Kuo CH, Chen CC, Su GD. Design, fabrication, and metrology of ultra-precision optical freeform surface for progressive addition lens with *B*-spline description. *Int J Adv Manuf Technol* 2012;63:225–33.
- [11] Wang J, Gulliver R, Santosa F. Analysis of a variational approach to progressive lens design. *SIAM J Appl Math* 2003;64:277–96.
- [12] Wang J, Gulliver R, Santosa F. Multifocal optical device design. US Patent 2005. 656690.